International Journal of Rotating Machinery
1998, Vol. 4, No. 2, pp. 73–90
Reprints available directly from the publisher
Photocopying permitted by license only

Two-Dimensional Convection Induced by Gravity and Centrifugal Forces in a Rotating Porous Layer Far Away from the Axis of Rotation

PETER VADASZ* and SANESHAN GOVENDER

Department of Mechanical Engineering, University of Durban-Westville, Private Bag X54001, Durban 4000, South Africa

(Received 9 December 1996)

The stability and onset of two-dimensional convection in a rotating fluid saturated porous layer subject to gravity and centrifugal body forces is investigated analytically. The problem corresponding to a layer placed far away from the centre of rotation was identified as a distinct case and therefore justifying special attention. The stability of a basic gravity driven convection is analysed. The marginal stability criterion is established in terms of a critical centrifugal Rayleigh number and a critical wave number for different values of the gravity related Rayleigh number. For any given value of the gravity related Rayleigh number there is a transitional value of the wave number, beyond which the basic gravity driven flow is stable. The results provide the stability map for a wide range of values of the gravity related Rayleigh number, as well as the corresponding flow and temperature fields.

Keywords: Rotating flows, Rotating machinery, Porous media, Free convection, Natural convection, Buoyancy

INTRODUCTION

The study of transport phenomena in rotating porous media is motivated by its practical applications in engineering and geophysics (Vadasz [1993a,b], [1996a]). The effect of rotation and of free convection as a result of the centrifugal and gravity body forces is of particular interest from both the practical and theoretical points of view. To mention only a few engineering applications let us consider the food process industry, chemical process industry and rotating machinery.

More specifically, packed bed mechanically agitated vessels are used in the food processing and chemical engineering industries in batch processes. The packed bed consists of solid particles or fibbers of material which form the solid matrix while fluid flows through the pores. As the solid matrix rotates, due to the mechanical agitation, a rotating frame of reference is a necessity

* Corresponding author.

when investigating these flows. The role of the flow of fluid through these beds can vary from drying processes to extraction of soluble components from the solid particles. The molasses in centrifugal crystal separation processes in the sugar milling industry and the extraction of sodium alginate from kelp are just two examples of such processes.

Modelling of flow and heat transfer in porous media is also applied for the design of heat pipes using porous wicks and includes effects of boiling in unsaturated porous medium, surface tension driven flow with heat transfer and condensation in unsaturated porous media. When the heat pipe is used for cooling devices which are subject to rotation the corresponding centrifugal and Coriolis effects become relevant as well.

The macro-level porous media approach is gaining an increased level of interest in solving practical fluid flow an heat transfer problems which are too difficult to solve by using a traditional micro-level approach. Some applications of the porous medium approach are discussed by Nield and Bejan [1992] and Bejan [1995] in comprehensive reviews of the fundamentals of heat convection in porous media. Bejan [1995] mentions among the applications of heat transfer in porous media the process of cooling of winding structures in high-power density electric machines. When this applies to a rotor of an electric machine, say generator (or motor), rotation effects become relevant as well.

A regenerator in a power plant can also be modelled by using the macro-level porous media approach. As the regenerator is typically subject to rotation the centrifugal effects on heat transfer are to be investigated.

With the emerging utilisation of the porous medium approach in non-traditional fields, including some applications in which the solid matrix is subjected to rotation, as well as the more established porous media applications a thorough understanding of the flow in a rotating porous medium becomes essential.

Research results (Patil and Vaidyanathan [1983], Jou and Liaw [1987a,b], Rudraiah, Shivakumara and Friedrich [1986] and Palm and Tyvand [1984]) are available for free convection in rotating porous media resulting from *gravity* in the presence of a single fluid or binary mixture. However, when a rotating porous matrix is considered, an additional body force exists in the form of the *centrifugal acceleration*. This force may generate free convection in the same manner as the gravity force causes natural convection. Vadasz [1993a] presented an analytical solution to the three-dimensional free convection problem in a long rotating porous box for the case when the temperature gradient resulting from the imposed conditions on the boundary is perpendicular to the centrifugal body force. The analysis focused on the effect of the Coriolis force on the basic free convection solution, for high values of Ekman number. Secondary circulation was obtained in a plane perpendicular to the leading free convection plane as a result of the Coriolis effect on the flow. Analytical solutions for the stability of free convection in a porous layer subject to rotation for the case when the temperature gradient resulting from the conditions imposed on the boundaries is collinear with the centrifugal body force were presented by Vadasz [1994] for a layer adjacent to the axis of rotation and by Vadasz [1996a] for a porous layer placed an arbitrary positive distance from the axis of rotation, where a singularity in the solution associated with negative values of the offset distance from the axis of rotation was identified. As this singularity occurs at negative values of the offset distance from the axis of rotation it implies that the location of the rotation axis falls within the boundaries of the porous domain (or to the left side of the cold wall – a case of little interest due to its inherent unconditional stability). This particular location of the rotation axis causes an alternating direction of the centrifugal body force within the porous layer. The results of a study investigating this particular configuration were presented by Vadasz [1996b]. These studies accounted for the effect of the centrifugal body force while neglecting the effect of gravity.

The objective of the present investigation is to establish the *combined effect of gravity and*

centrifugal acceleration, as body forces, on free convection in a porous layer.

PROBLEM FORMULATION

A narrow fluid saturated porous layer subject to rotation is placed a dimensionless distance x_0 from the centre of rotation as presented in Fig. 1. The offset distance is presented in a dimensionless form representing the ratio between the dimensional offset distance and the length of the porous layer in the form $x_0 = x_{0*}/L_*$. Two systems of coordinates are presented in Fig. 1, the first (x', y', z') is linked to the axis of rotation and the second (x, y, z), placed a horizontal distance x_0 apart from the first one, belongs to the porous layer coordinates. A positive temperature gradient in the x direction is anticipated as a result of the imposed thermal boundary conditions. This temperature gradient is collinear with the centrifugal acceleration and perpendicular to the gravity acceleration. The significance of the variation of the centrifugal acceleration in the x direction depends on the offset distance from the centre of rotation. For the layer which is adjacent to the rotation axis (i.e., $x_0 = 0$) the variation of the centrifugal acceleration leads practically to a zero acceleration at $x = 0$ and a maximum value of acceleration at $x = 1$. However, for the layer which is far away from the rotation axis ($x_0 \gg 1$) the centrifugal acceleration is almost constant. The front aspect ratio of the layer is defined as $H = H_*/L_*$ where H_* and L_* are the height and the length of the layer respectively. The top aspect ratio is $W = W_*/L_*$ where W_* is the width of the layer. The following analysis is confined to a narrow and very tall layer, i.e. $W \ll 1$ and $H \gg 1$. A basic free convection flow occurs unconditionally as a result of the gravity acceleration. Related to the gravity acceleration this convection is practically the case of differentially heating a porous layer from the sides. The only inertial effect considered is the centrifugal acceleration, as far as changes in density are concerned. Other than that the Darcy's law is assumed to govern the fluid flow (extended to include the centrifugal acceleration), while the Boussinesq approximation is applied for the effects of density variations. As a narrow layer is considered, i.e. $W \ll 1$, a Cartesian coordinate system can be used and the component of the centrifugal acceleration in the y direction can be neglected. Under these conditions the following dimensionless set of governing equations is obtained

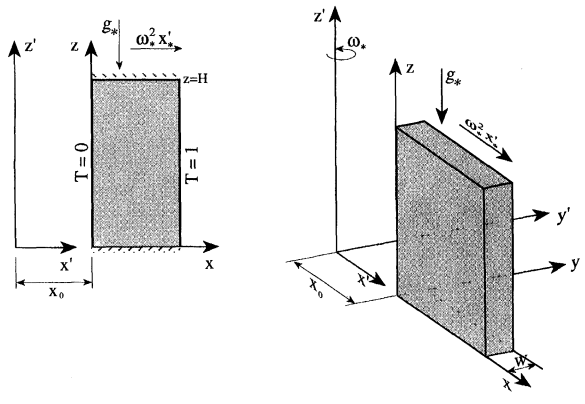

FIGURE 1 A rotating fluid saturated porous layer subject to different temperatures at the sidewalls.

$$\nabla \cdot \boldsymbol{q} = 0, \tag{1}$$

$$\boldsymbol{q} = -\nabla p - [Ra_{\omega 0} + Ra_{\omega} x] T \hat{\boldsymbol{e}}_x + Ra_g T \hat{\boldsymbol{e}}_z, \tag{2}$$

$$\frac{\partial T}{\partial t} + \boldsymbol{q} \cdot \nabla T = \nabla^2 T. \tag{3}$$

Equations (1)–(3) are presented in a dimensionless form. The values $\alpha_{e*}/L_* M_f$, $\mu_* \alpha_{e*}/k_* M_f$, and $\Delta T_c = (T_H - T_C)$ are used to scale the filtration velocity components (u_*, v_*, w_*), pressure (p_*), and temperature variations $(T_* - T_C)$, respectively, where α_{e*} is the effective thermal diffusivity, μ_* is the fluid's viscosity, k_* is the permeability of the porous matrix and M_f is the ratio between the heat capacity of the fluid and the effective heat capacity of the porous domain. The length of the layer L_* was used for scaling the variables x_*, y_* and z_*. Accordingly, $x = x_*/L_*$, $y = y_*/L_*$ and $z = z_*/L_*$. The

gravity related Rayleigh number is defined in Eq. (2) as $Ra_g = \beta_* \Delta T_c g_* L_* k_* M_f / \alpha_{e*} \nu_*$. In Eq. (2) one observes also two different centrifugal Rayleigh numbers; $Ra_{\omega 0} = \beta_* \Delta T_c \omega_*^2 x_{0*} L_* \, k_* M_f / \alpha_{e*} \nu_*$ is the centrifugal Rayleigh number representing the contribution of the offset distance from the rotation centre to the centrifugal acceleration and $Ra_\omega = \beta_* \Delta T_c \omega_*^2 L_*^2 k_* M_f / \alpha_{e*} \nu_*$ represents the contribution of the horizontal location within the porous layer to the centrifugal acceleration. It is convenient for the following analysis to introduce the ratio between the two centrifugal Rayleigh numbers as a parameter in the equations in the form

$$\eta = \frac{Ra_\omega}{Ra_{\omega 0}} = \frac{1}{x_0}. \tag{4}$$

This ratio, representing also the reciprocal of the dimensionless offset distance from the centre of rotation, can be introduced into Eq. (2) to obtain

$$\boldsymbol{q} = -\nabla p - Ra_{\omega 0}[1 + \eta x] T \hat{\boldsymbol{e}}_x + Ra_g T \hat{\boldsymbol{e}}_z. \tag{5}$$

From Eq. (5) it is observed that when the porous layer is far away from the centre of rotation then $\eta \ll 1$ ($x_0 \gg 1$) and the contribution of the term ηx is not significant, while for a layer close enough to the rotation centre $\eta \gg 1$ ($x_0 \ll 1$) and the contribution of the first term becomes insignificant. In the first case the only controlling parameter is $Ra_{\omega 0}$ while in the later case the only controlling parameter is $Ra_\omega = \eta Ra_{\omega 0}$.

As all the boundaries are rigid, the solution must follow the impermeability conditions there, i.e. $\boldsymbol{q} \cdot \hat{\boldsymbol{e}}_n = 0$ on the boundaries, where $\hat{\boldsymbol{e}}_n$ is a unit vector normal to the boundary. The temperature boundary conditions are: $T = 0$ at $x = 0$, $T = 1$ at $x = 1$ and $\nabla T \cdot \hat{\boldsymbol{e}}_n = 0$ on all other walls representing the insulation condition on these walls.

The partial differential equations (1), (3) and (5) form a non-linear coupled system which together with the corresponding boundary conditions accepts a basic gravity driven convection solution. The establishment of the conditions of stability of this basic solution is the objective of this analysis.

METHOD OF SOLUTION

For a very tall porous layer the basic gravity driven convection solution far from the top and bottom end-walls is presented in the form

$$\begin{aligned} &u_b = v_b = 0, \quad w_b = Ra_g(x - 1/2), \quad T_b = x, \\ &p_b = 1/2 Ra_g z - Ra_{\omega 0}[x^2/2 + \eta x^3/3] + \text{const.} \end{aligned} \tag{6}$$

This solution satisfies the governing equations and the boundary conditions. Therefore the solution is presented as the sum of this *basic solution* and *small perturbations* in the form

$$\boldsymbol{q} = \boldsymbol{q}_b + \boldsymbol{q}', \quad T = T_b + T', \quad p = p_b + p', \tag{7}$$

where the ($'$) stands for perturbed values. Substituting Eqs. (6) and (7) into the governing equations (1), (3) and (5), and linearising the result by neglecting terms which include products of perturbations which are small, yields the following set of linear partial differential equations for the perturbations

$$\nabla \cdot \boldsymbol{q}' = 0, \tag{8}$$

$$\boldsymbol{q}' = -\nabla p' - Ra_{\omega 0}[1 + \eta x] T' \hat{\boldsymbol{e}}_x + Ra_g T' \hat{\boldsymbol{e}}_z, \tag{9}$$

$$\left[\frac{\partial}{\partial t} - \nabla^2\right] T' + u' + Ra_g(x - 1/2)\frac{\partial T'}{\partial z} = 0. \tag{10}$$

Applying twice the *curl* operator on Eq. (9) and using the property of $\boldsymbol{q}'$ being a solenoidal vector which comes out from Eq. (8), yields

$$\begin{aligned} \nabla^2 \boldsymbol{q}' = &\left\{ Ra_{\omega 0}\left[-(1 + \eta x)\left(\frac{\partial^2 T'}{\partial y^2} + \frac{\partial^2 T'}{\partial z^2}\right)\right] \right. \\ &\left. - Ra_g\left[\frac{\partial^2 T'}{\partial x \partial z}\right]\right\} \hat{\boldsymbol{e}}_x \\ &+ \left\{ Ra_{\omega 0}\left[(1 + \eta x)\frac{\partial^2 T'}{\partial x \partial y} + \eta \frac{\partial T'}{\partial y}\right] \right. \\ &\left. - Ra_g\left[\frac{\partial^2 T'}{\partial y \partial z}\right]\right\} \hat{\boldsymbol{e}}_y \\ &+ \left\{ Ra_{\omega 0}\left[(1 + \eta x)\frac{\partial^2 T'}{\partial x \partial z} + \eta \frac{\partial T'}{\partial z}\right] \right. \\ &\left. + Ra_g\left[\frac{\partial^2 T'}{\partial x^2} + \frac{\partial^2 T'}{\partial y^2}\right]\right\} \hat{\boldsymbol{e}}_z. \end{aligned} \tag{11}$$

The horizontal x component of Eq. (11) is sufficient for solving Eq. (10), i.e.,

$$\nabla^2 u' + \left\{ Ra_{\omega 0}(1+\eta x)\left[\frac{\partial^2}{\partial y^2}+\frac{\partial^2}{\partial z^2}\right] + Ra_g\left[\frac{\partial^2}{\partial x \partial z}\right]\right\} T' = 0. \tag{12}$$

The coupling between Eqs. (10) and (12) can be resolved leading to one equation for the temperature perturbations in the form

$$\left[\left(\frac{\partial}{\partial t} - \nabla^2 + Ra_g(x-1/2)\frac{\partial}{\partial z}\right)\nabla^2 + Ra_g \frac{\partial^2}{\partial x \partial z} - Ra_{\omega 0}(1+\eta x)\left(\frac{\partial^2}{\partial y^2}+\frac{\partial^2}{\partial z^2}\right)\right] T' = 0. \tag{13}$$

Assuming an expansion into normal modes in the y and z directions, i.e., $T' = A_\kappa \theta(x) \times \exp[\sigma t + i(\kappa_y y + \kappa_z z)]$ yields the following ordinary differential equation for θ

$$\{(D^2 - \kappa^2 - \sigma)(D^2 - \kappa^2) - Ra_{\omega 0}(1+\eta x)\kappa^2 - i\kappa_z Ra_g[(x-1/2)(D^2-\kappa^2) + D]\}\theta = 0. \tag{14}$$

where $D \equiv d/dx$, $\kappa^2 = \kappa_y^2 + \kappa_z^2$ and κ_y, κ_z are the wave numbers in the y and z directions respectively.

The Galerkin method is adopted to solve Eq. (14). Consequently $\theta(x)$ is expanded in a series of orthogonal trial functions $\phi_m(x)$ which satisfy the boundary conditions in the form

$$\theta(x) = \sum_{m=1}^{M} a_m \phi_m(x). \tag{15}$$

At marginal stability $\sigma = 0$ and upon substitution of expansion (15) into Eq. (14) one can multiply the resulting equation by $\phi_l(x)$ and integrate over the length of the domain. In the particular case considered here the choice $\phi_m = \sin(m\pi x)$ proved to be a trial function which satisfies the necessary conditions. Upon substitution of this trial function into Eq. (15), introducing the results into Eq. (14), multiplying the resulting equation by $\phi_l = \sin(l\pi x)$ and integrating over the length of the domain one obtains a homogeneous set of linear algebraic equations in the form

$$\sum_{m=0}^{M} \left\{ \left[(m^2+\alpha)^2 - \alpha\left(1+\frac{\eta}{2}\right)R_{\omega 0}\right]\delta_{ml} + \left[\frac{4\alpha\eta R_{\omega 0} ml}{(m^2-l^2)^2\pi^2}\right]\delta_{m+l,2p-1} - i\gamma R_g \left[\frac{4ml}{(m^2-l^2)^2\pi^2} \times [(m^2+l^2)+2\alpha]\right]\delta_{m+l,2p-1}\right\} a_m = 0 \tag{16}$$

for $l = 1, 2, 3, \ldots, M$, where the following scaling and notation was introduced for convenience

$$\alpha = \frac{\kappa^2}{\pi^2};\ \gamma = \frac{\kappa_z}{\pi};\ R_{\omega 0} = \frac{Ra_{\omega 0}}{\pi^2};\ R_g = \frac{Ra_g}{\pi}. \tag{17}$$

In Eq. (16) δ_{ml} is the Kronecker delta function and the index p can take arbitrary integer values; it stands only for setting the second index in the Kronecker delta function to be an odd integer. The particular interest on two-dimensional solutions in the x–z plane limits the results to the case when the layer is placed far away from the centre of rotation corresponding to $\eta = 0$ (i.e. $x_0 \to \infty$). All other results yield at least two-dimensional solutions in the y–z plane at the perturbation level, which eventually become three-dimensional when combined with the basic solution. Therefore for the case of interest covered in this paper we substitute $\eta = 0$ in Eq. (16) to obtain

$$\sum_{m=1}^{M} \left\{ [(m^2+\alpha)^2 - \alpha R_{\omega 0}]\delta_{ml} - i\gamma R_g \times \left[\frac{4ml}{(m^2-l^2)^2\pi^2}[(m^2+l^2)+2\alpha]\right]\delta_{m+l,2p-1}\right\} a_m = 0. \tag{18}$$

Equation (18) has the form $\mathbb{L}(a_m) = 0$, representing a homogeneous linear system accepting a non-zero solution only for particular values of $R_{\omega 0}$ such that **det** $[\mathbb{L}(a_m)] = 0$.

RESULTS AND DISCUSSION

Although the research on these values of $R_{\omega 0}$ and more particularly on the critical ones, has been done by solving (18) up to the rank $M=10$ for different values of R_g, useful information can be drawn by considering the approximation to rank $M=2$. For this rank of approximation the system reduces to two equations which are expressed in the following matrix representation

$$\begin{bmatrix} [(1+\alpha)^2-\alpha R_{\omega 0}]; & [-i8\gamma R_g(5+2\alpha)/9\pi^2] \\ [-i8\gamma R_g(5+2\alpha)/9\pi^2]; & [(4+\alpha)^2-\alpha R_{\omega 0}] \end{bmatrix} \times \begin{bmatrix} a_1 \\ a_2 \end{bmatrix} = 0. \tag{19}$$

Taking the determinant of (19) and equating it to zero leads to the characteristic values of $R_{\omega 0}$ in the form

$$R_{\omega 0,c} = \frac{[(1+\alpha)^2+(4+\alpha)^2]}{2\alpha} \pm \frac{(5+2\alpha)\sqrt{(27\pi^2)^2-(16\gamma R_g)^2}}{18\pi^2\alpha}. \tag{20}$$

It can be observed that this equation will no longer yield a real solution for $R_{\omega 0,c}$ if the discriminant is negative, i.e. if $(16\gamma R_g)^2 > (27\pi^2)^2$. For the particular two-dimensional problem, i.e. the case corresponding to the solution in the x–z plane, the following relationships hold: $\kappa_y^2 = 0 \Rightarrow \kappa^2 = \kappa_z^2$ and $\alpha = (\kappa^2/\pi^2) = (\kappa_z^2/\pi^2) = \gamma^2$. Introducing these relationships into Eq. (20) yields

$$R_{\omega 0,c} = \frac{[(1+\alpha)^2+(4+\alpha)^2]}{2\alpha} \pm \frac{(5+2\alpha)\sqrt{(27\pi^2)^2-\alpha(16R_g)^2}}{18\pi^2\alpha} \tag{21}$$

and this equation will no longer yield real solutions for $R_{\omega 0,c}$ if $\alpha(16R_g)^2 > (27\pi^2)^2$. For the equation to yield real solutions, the following condition has to be fulfilled

$$\alpha < \left(\frac{27\pi^2}{16R_g}\right)^2. \tag{22}$$

In other words, for any value of R_g there is a transitional value of α, say α_{tr} such that $\alpha < \alpha_{tr}$ in order for the solution of $R_{\omega 0,c}$ to be real. This transitional value of α is taken from Eq. (22) to be $\alpha_{tr} = (27\pi^2/16R_g)^2$. In turn, this result defines the corresponding transitional wave number κ_{tr}. The physical interpretation of this transitional value of κ is that beyond this value the basic gravity driven convective flow is stable. The expression for $R_{\omega 0,c}$ was evaluated as a function of κ for different values of R_g at rank $M=2$ and its accuracy was confirmed by evaluating the characteristic values to higher ranks up to $M=10$ by using *Mathematica*™, Wolfram [1991] for symbolic as well as numerical computations. The results are presented graphically in Fig. 2. The minima on the curves correspond to the critical values of $Ra_{\omega 0}$. It can be observed from the figure that for any value of Ra_g there is a transitional value of κ beyond which no real values of $Ra_{\omega 0,c}$ exist. Connecting these points on the $(Ra_{\omega 0,c}/\pi^2 - \kappa/\pi)$ plane yields a curve indicating that points above it represent a case when the basic gravity driven convective flow is stable. This is represented by the grey curve in Fig. 2 providing a top boundary for the stability curves. The stability curve corresponding to $Ra_g = 0$ provides the bottom boundary. Therefore, all the stability curves for different values of Ra_g will be located in-between these two extreme curves, forming an envelope for the stability curves.

The critical and transitional values of the wave number, represented by the values of κ corresponding to the minima on the curves in Fig. 2 and by κ_{tr} as a function of Ra_g, are presented graphically in Fig. 3(a). The figure shows that the transitional wave number is greater than the critical wave number for all values of Ra_g considered. By using the transitional value of α $(=\kappa/\pi)$ from Eq. (22) and taking the log, yields

$$\log\left(\frac{\kappa_{tr}}{\pi}\right) = \log\left(\frac{27\pi^2}{16}\right) - \log\left(\frac{Ra_g}{\pi}\right). \tag{23}$$

Equation (23) shows that the relationship between the transitional wave number and the gravity related Rayleigh number is represented

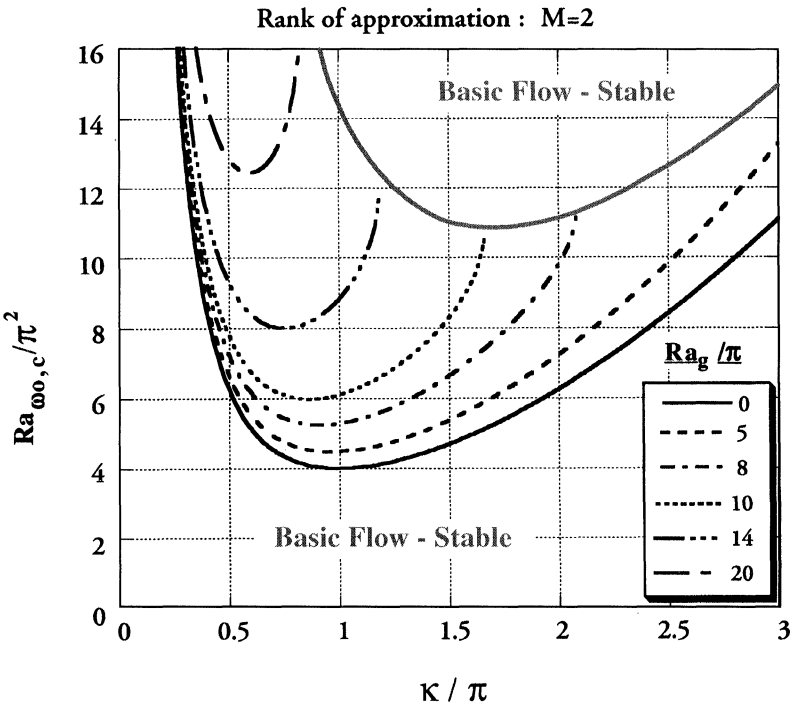

FIGURE 2 The characteristic curves representing the marginal stability and the transitional limit for different values of the Gravity related Rayleigh number at rank 2 of approximation.

by a straight line on a log–log diagram, at rank 2 of approximation. This linear relationship is presented graphically in Fig. 3(b).

The critical values of the centrifugal Rayleigh number, at rank 2, represented by the minima of $Ra_{\omega 0,c}$ on the curves in Fig. 2, are presented as function of Ra_g in Fig. 4, in comparison with the corresponding critical values as evaluated at rank 10. From Fig. 4 it can be observed that the discrepancy between the results at rank 2 and at rank 10 is small for moderate and small values of (Ra_g/π). As the values of the gravity related Rayleigh number increase the more accurate rank 10 results deviate significantly from the lower rank $(M=2)$ values. The more accurate transitional values of the wave number as evaluated at rank 10 are presented graphically as a function of (Ra_g/π) in Fig. 5(a) together with the corresponding rank 10 results of the critical wave number. The tendency observed at rank 2, that $\kappa_{tr} > \kappa_{cr}$ over the range of Ra_g considered, is retained at rank 10 as well. The detail of the curve representing the critical wave number as a function of the gravity related Rayleigh number at rank 10 is presented in Fig. 5(b). It is observed from the figure that the wave number decreases initially, reaches a local minimum followed by an increase, and stabilises eventually at a value of κ_{cr}/π slightly less than 0.9, not before passing through an overshooting behaviour. This non-monotonic shape of the critical wave number as a function of a parameter (in this case Ra_g) is quite unusual and it was verified in a few different ways to confirm its pattern.

The results can now be used to evaluate the ratio between the coefficients in the series (15). As the linear stability does not allow for the evaluation of the amplitude of the convection, the coefficient a_1 can be absorbed in the definition of the amplitude A, therefore leaving in the series the ratios $b_m = a_m/a_1 \; \forall m = 1, 2, \ldots, M$ where $b_1 = 1$ by definition. These coefficients were evaluated up to $M = 10$. Then for convective rolls having axes parallel to

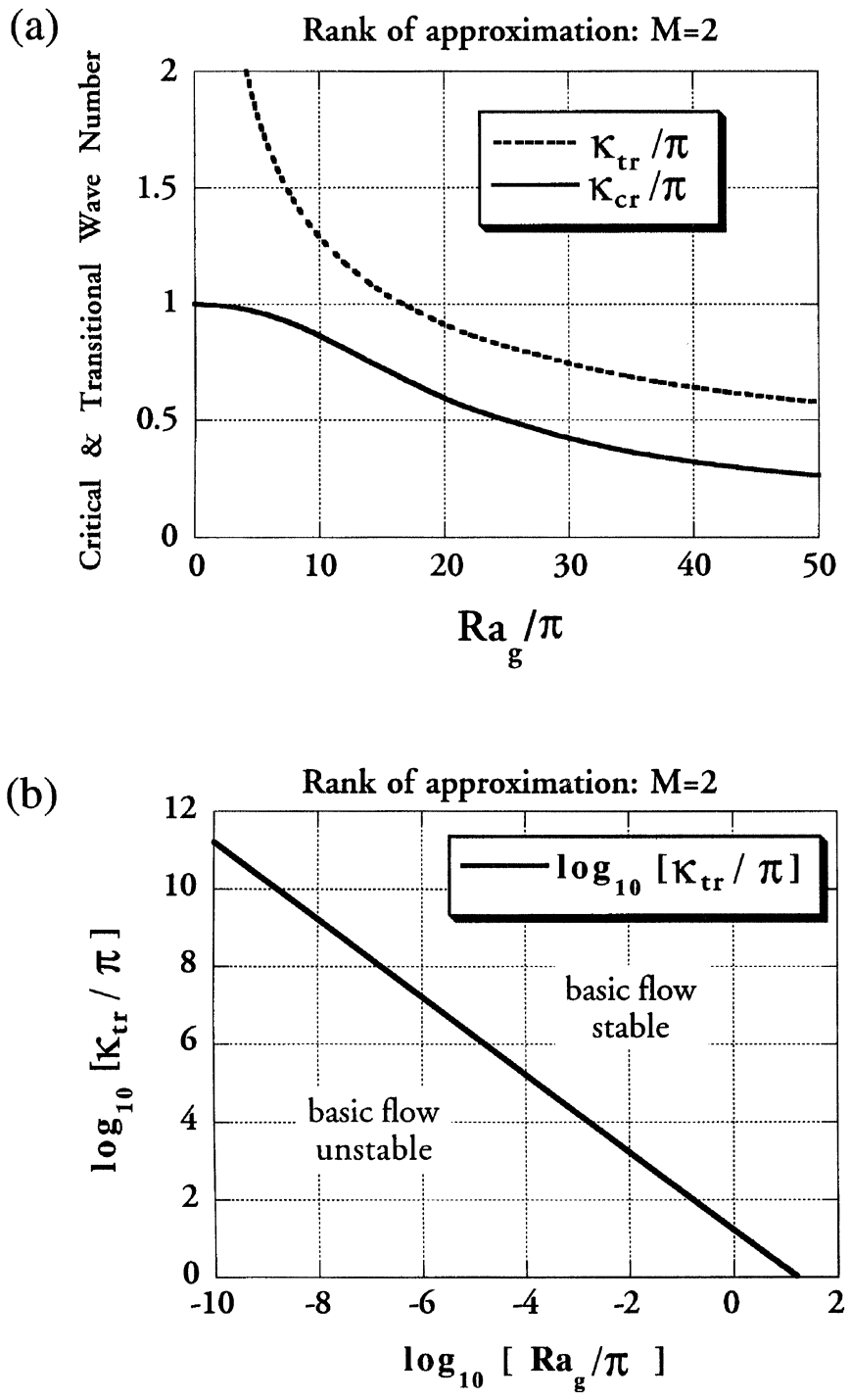

FIGURE 3 The variation of the critical and transitional values of the wave number as a function of the Gravity related Rayleigh number at rank 2 of approximation; (a) Critical and transitional values of κ versus Ra_g. (b) Transitional values of κ versus Ra_g on a log–log scale showing a straight line on this scale.

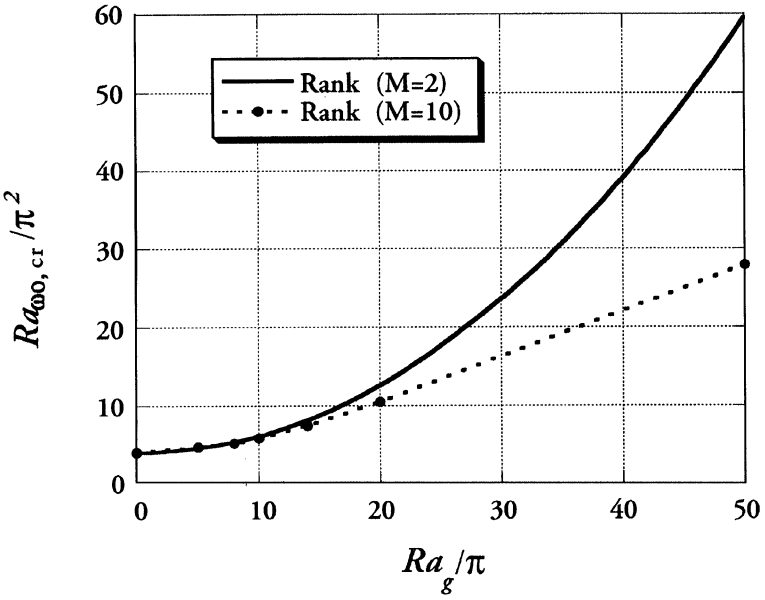

FIGURE 4 The variation of the critical values of the Centrifugal Rayleigh number as a function of the Gravity related Rayleigh number; a comparison between results at ranks 2 and 10.

the shorter dimension (i.e. y) the eigenfunctions were evaluated and can be expressed in the form

$$T' = A_r \cos\left(\frac{n\pi z}{H}\right) \sum_{m=1}^{M} b_{2m-1} \sin[(2m-1)\pi x] + iA_i \cos\left(\frac{n\pi z}{H}\right) \sum_{m=1}^{M} b_{2m} \sin[2m\pi x]. \quad (24)$$

Since the even coefficients in the series, i.e. the values of b_m corresponding to $m = 2, 4, 6, 8, \ldots$, are imaginary constants at all ranks, the series had to be presented by separating the odd modes from the even modes as observed in Eq. (24). As the flow is two-dimensional, a stream function can be used for presenting the results graphically. The stream function was evaluated and is expressed in the form

$$\psi' = -A_r \left[\frac{H}{n\pi} \sin\left(\frac{n\pi z}{H}\right) \sum_{m=1}^{M} b_{2m-1} \left[\frac{n^2}{H^2} + (2m-1)^2\right] \times \pi^2 \sin[(2m-1)\pi x] + Ra_g(x - 1/2) \times \cos\left(\frac{n\pi z}{H}\right) \sum_{m=1}^{M} b_{2m-1} \sin[(2m-1)\pi x] \right]$$

$$- iA_i \left[\frac{H}{n\pi} \sin\left(\frac{n\pi z}{H}\right) \sum_{m=1}^{M} b_{2m} \left[\frac{n^2}{H^2} + 4m^2\right] \times \pi^2 \sin[2m\pi x] + Ra_g(x - 1/2) \times \cos\left(\frac{n\pi z}{H}\right) \sum_{m=1}^{M} b_{2m} \sin[2m\pi x] \right]. \quad (25)$$

In Eqs. (24) and (25) $(n\pi/H)$ represents the wave number κ and in all calculations pertaining to the presentation of the results the following amplitude relationship was used $A_r = -A_i = A$.

Finally, the complete solution for the temperature in terms of isotherms T and for the flow field in terms of the stream function ψ, is presented in the form

$$T = T_b + T'; \qquad \psi = \psi_b + \psi', \quad (26)$$

where T' is given by Eq. (24), ψ' is given by Eq. (25), $T_b = x$ is taken from Eq. (6) and ψ_b was evaluated from Eq. (6) for w_b, in the form

$$\psi_b = -\frac{Ra_g}{2} x(x-1). \quad (27)$$

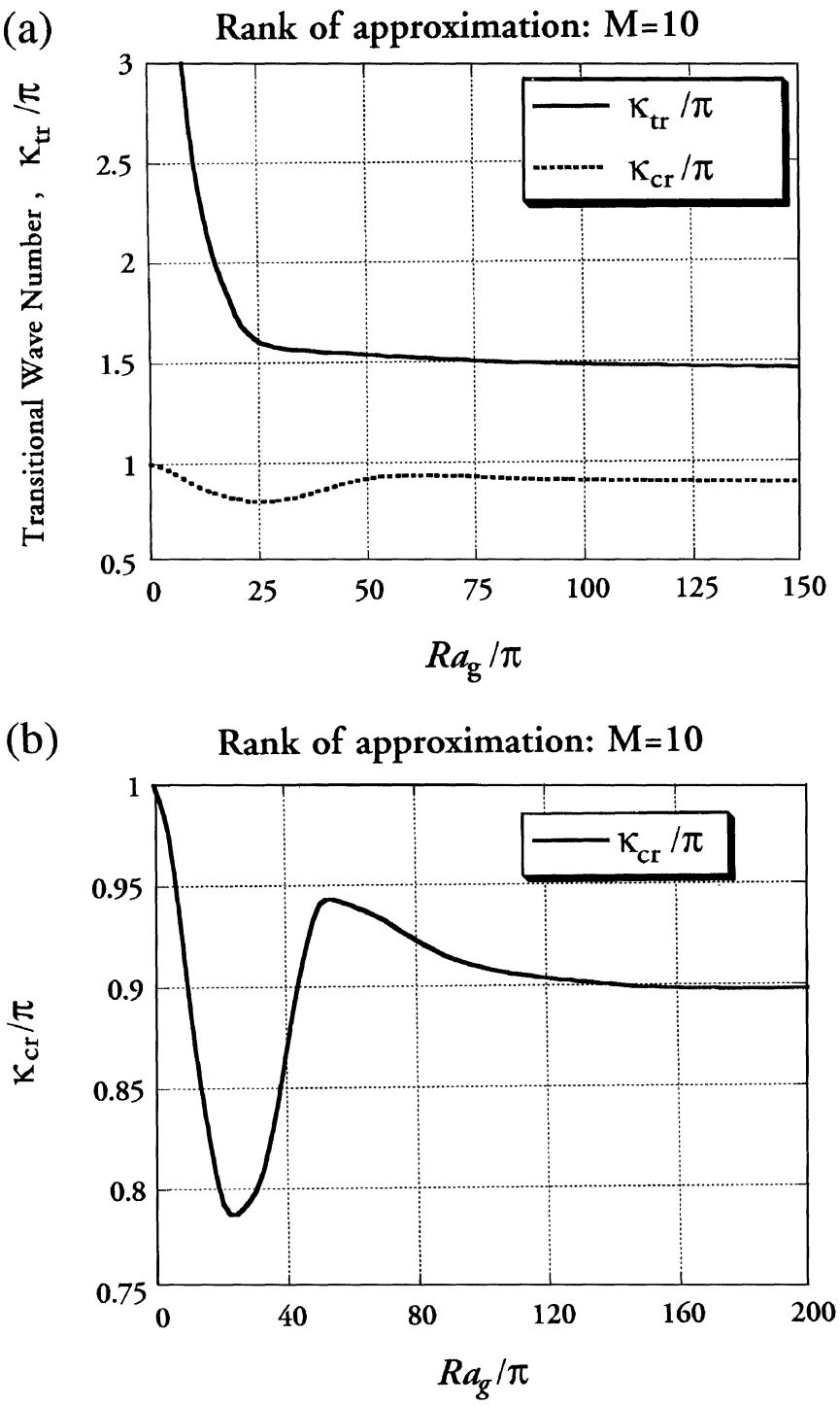

FIGURE 5 The variation of the critical and transitional values of the wave number as a function of the Gravity related Rayleigh number at rank 10 of approximation; (a) Critical and transitional values of κ versus Ra_g. (b) Critical values of κ versus Ra_g (detail).

The results of the convective flow field for an amplitude of $A = 0.2$ are presented graphically in Fig. 6 for four moderate values of Ra_g/π, corresponding to the odd modes. From the figure it can be observed that the effect of increasing the gravity related Rayleigh number appears in the form of a tilt of the convection cells. The higher the value of Ra_g/π, the higher the tilt angle. At $(Ra_g/\pi) = 0$ there is no basic convection (the basic solution is motionless) hence the only flow occurs as a result of the centrifugal driven convection at the perturbation level. However as soon as the value of Ra_g/π increases one can observe the basic flow upwards next to the hot sidewall and downwards next to the cold sidewall, and secondary convection cells filling the space in-between. As the value of Ra_g/π increases the basic flow moves towards the interior and leaves less space for the secondary cells, providing the major reason for the tilt angle of the convection cells. This effect becomes more pronounced for high values of Ra_g/π as can be observed in Fig. 7. The secondary flow cells become longer and their tilt angle increases as the value of Ra_g/π increases. The corresponding results of the convective flow field corresponding to the even modes are presented graphically in Figs. 8 and 9. The results for moderate values of Ra_g/π are presented in Fig. 8 while the results for the high values of the parameter appear in Fig. 9. The common fact for the even modes convection results is that the flow is dominated by the basic solution while only a limited core section of the flow domain is significantly affected by the centrifugally driven convection. Although the meandering of the basic gravity driven flow is a

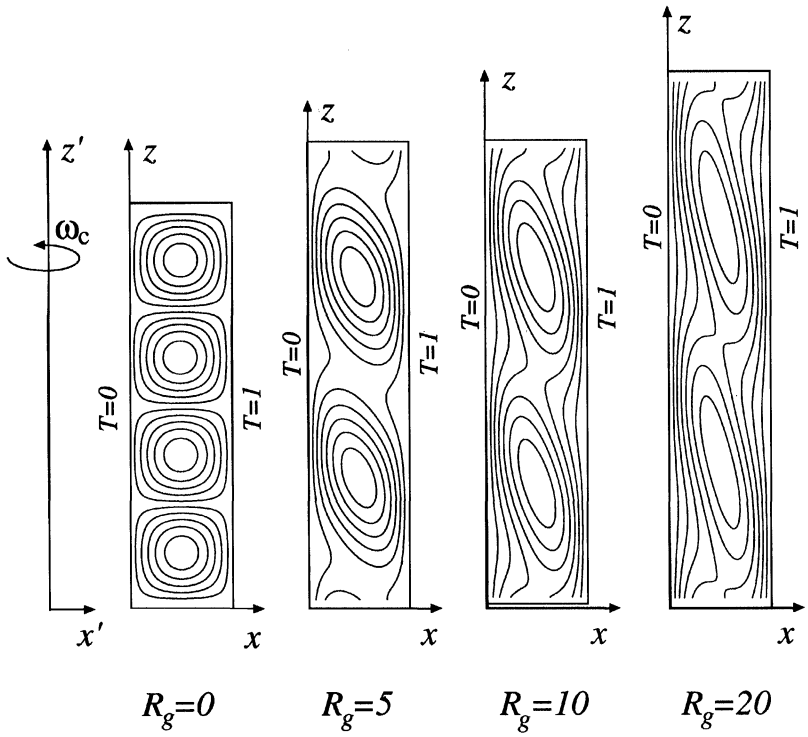

FIGURE 6 The convective flow field at marginal stability for the odd modes corresponding to $A = 0.2$ and to four different values of R_g; stream lines equally divided between ψ_{min} and ψ_{max}. For $R_g = 0$: $\psi_{min} = -1.257$; $\psi_{max} = 1.257$, for $R_g = 5$: $\psi_{min} = 0$; $\psi_{max} = 3.286$, for $R_g = 10$: $\psi_{min} = 0$; $\psi_{max} = 5.430$ and for $R_g = 20$: $\psi_{min} = 0$; $\psi_{max} = 9.937$.

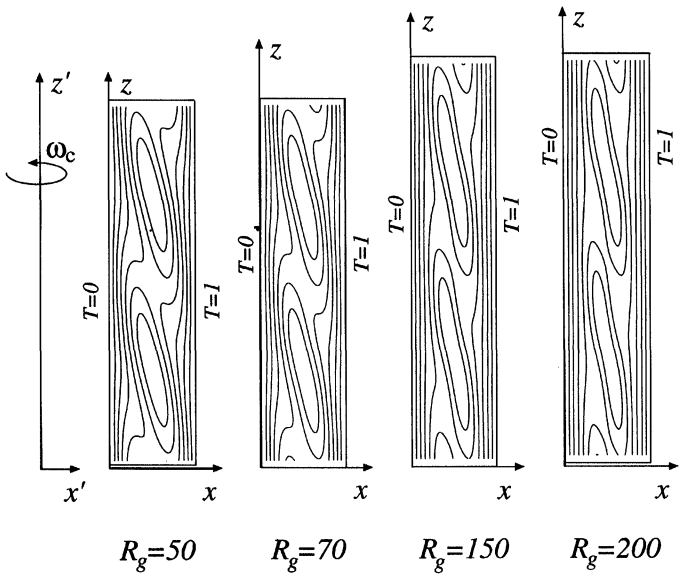

FIGURE 7 The convective flow field at marginal stability for the odd modes corresponding to $A=0.2$ and to four different values of R_g; stream lines equally divided between $\psi_{\min}$ and $\psi_{\max}$. For $R_g=50$: $\psi_{\min}=0$; $\psi_{\max}=24.381$, for $R_g=70$: $\psi_{\min}=0$; $\psi_{\max}=33.449$, for $R_g=150$: $\psi_{\min}=0$; $\psi_{\max}=70$ and for $R_g=200$: $\psi_{\min}=0$; $\psi_{\max}=93.023$.

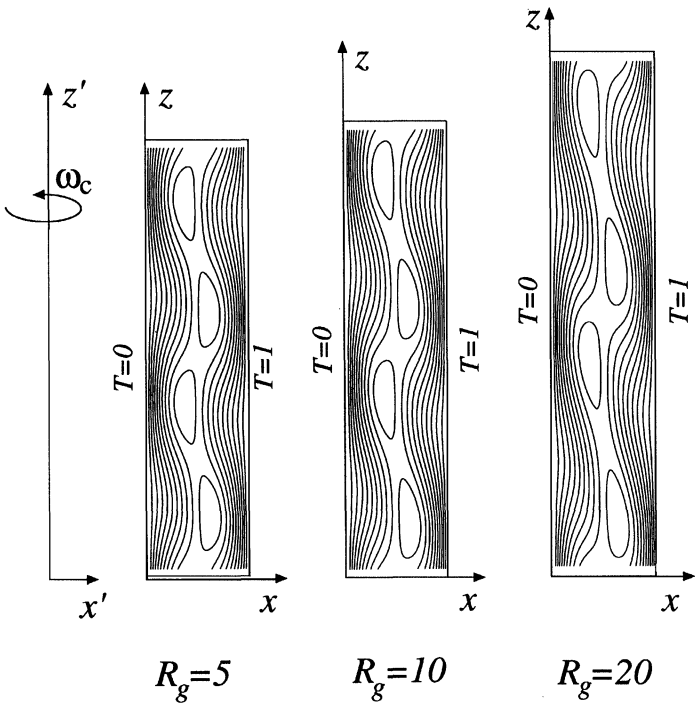

FIGURE 8 The convective flow field at marginal stability for the even modes corresponding to $A=0.2$ and to three different values of R_g; stream lines equally divided between $\psi_{\min}$ and $\psi_{\max}$. For $R_g=5$: $\psi_{\min}=0$; $\psi_{\max}=2.155$, for $R_g=10$: $\psi_{\min}=0$; $\psi_{\max}=4.322$ and for $R_g=20$: $\psi_{\min}=0$; $\psi_{\max}=8.739$.

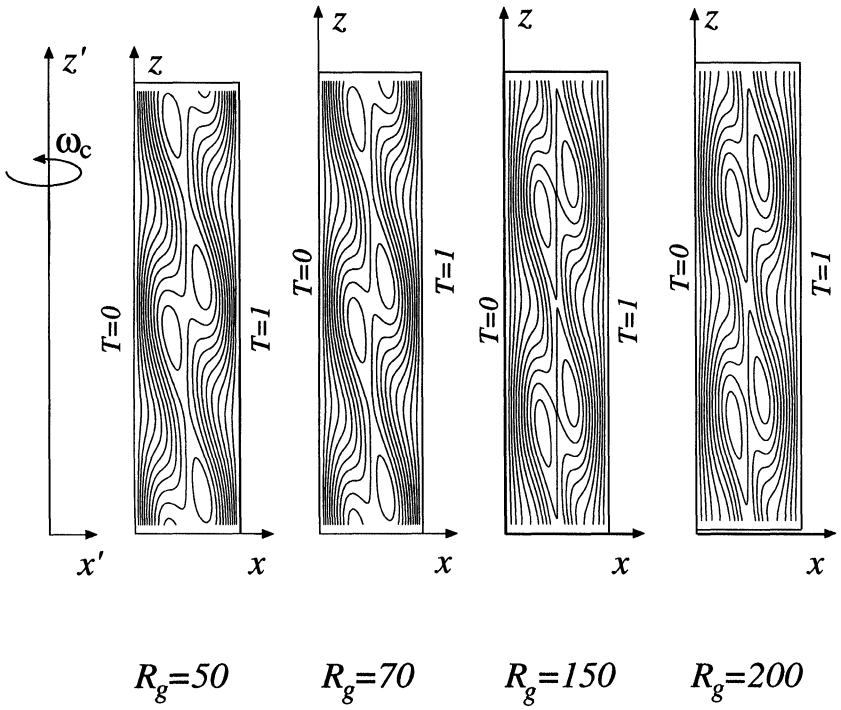

FIGURE 9 The convective flow field at marginal stability for the even modes corresponding to $A = 0.2$ and to four different values of R_g; stream lines equally divided between ψ_{min} and ψ_{max}. For $R_g = 50$: $\psi_{min} = 0$; $\psi_{max} = 23.146$, for $R_g = 70$: $\psi_{min} = 0$; $\psi_{max} = 32.506$, for $R_g = 150$: $\psi_{min} = 0$; $\psi_{max} = 70.672$ and for $R_g = 200$: $\psi_{min} = 0$; $\psi_{max} = 94.875$.

result of the centrifugal convection the latter has a more significant impact in the core where secondary cells appear. As the value of Ra_g/π increases any couple of two convection cells distant themselves from other couples but the cells within each couple get closer to each other. In order to analyse the impact of the amplitude of the centrifugal convection on the combined flow the results for an amplitude value of $A = 0.4$ are used to observe this effect graphically. Hence, the convective flow field for an amplitude of $A = 0.4$ are presented graphically in Fig. 10 for four moderate values of Ra_g/π, corresponding to the odd modes. From the figure it can be observed that at a value of $(Ra_g/\pi) = 5$ the flow is predominantly dominated by the centrifugal convection effect, while the only effect of the gravity driven basic flow is in providing the tilt of the convection cells. As the value of Ra_g/π increases the basic flow becomes more pronounced, increasing the tilt and controlling the flow next to the sidewalls. However, as can be observed from Fig. 11, for this higher amplitude of centrifugal convection, increasing the value of Ra_g/π further doesn't cause the basic flow to move to the interior, on the contrary, streamlines which bend towards the interior at values of $(Ra_g/\pi) = 50$ will eventually close and form tertiary convection cells at values of $(Ra_g/\pi) = 200$. The secondary flow cells become longer and their tilt angle increases as the value of Ra_g/π increases. The results for the isotherms corresponding to the moderate amplitude of $A = 0.2$ and to moderate values of Ra_g/π is presented in Fig. 12 for the odd modes and in Fig. 14 for the even modes. The striking effects of the combined gravitational and centrifugal convection on the temperature field appear, however, only at high values of the gravity related Rayleigh number, as presented graphically in Fig. 13 for the odd modes and in Fig. 15 for the even modes. Closed isotherms, representing temperature spots, appear in both

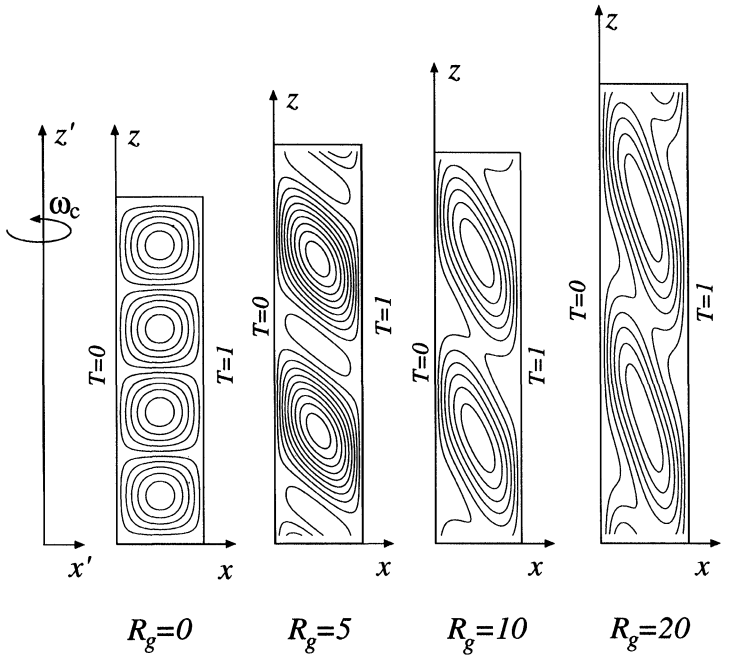

FIGURE 10 The convective flow field at marginal stability for the odd modes corresponding to $A = 0.4$ and to four different values of R_g; stream lines equally divided between $\psi_{\min}$ and $\psi_{\max}$. For $R_g = 0$: $\psi_{\min} = -2.558$; $\psi_{\max} = 2.558$, for $R_g = 5$: $\psi_{\min} = 0$; $\psi_{\max} = 3.926$, for $R_g = 10$: $\psi_{\min} = 0$; $\psi_{\max} = 6.887$ and for $R_g = 20$: $\psi_{\min} = 0$; $\psi_{\max} = 12.021$.

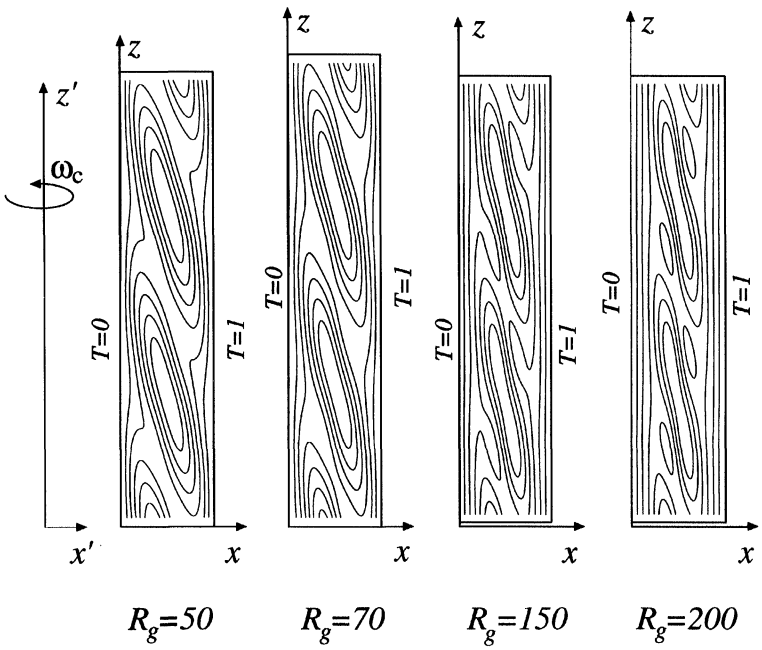

FIGURE 11 The convective flow field at marginal stability for the odd modes corresponding to $A = 0.4$ and to four different values of R_g; stream lines equally divided between $\psi_{\min}$ and $\psi_{\max}$. For $R_g = 50$: $\psi_{\min} = 0$; $\psi_{\max} = 29.129$, for $R_g = 70$: $\psi_{\min} = 0$; $\psi_{\max} = 39.573$, for $R_g = 150$: $\psi_{\min} = 0$; $\psi_{\max} = 82.315$ and for $R_g = 200$: $\psi_{\min} = 0$; $\psi_{\max} = 109.276$.

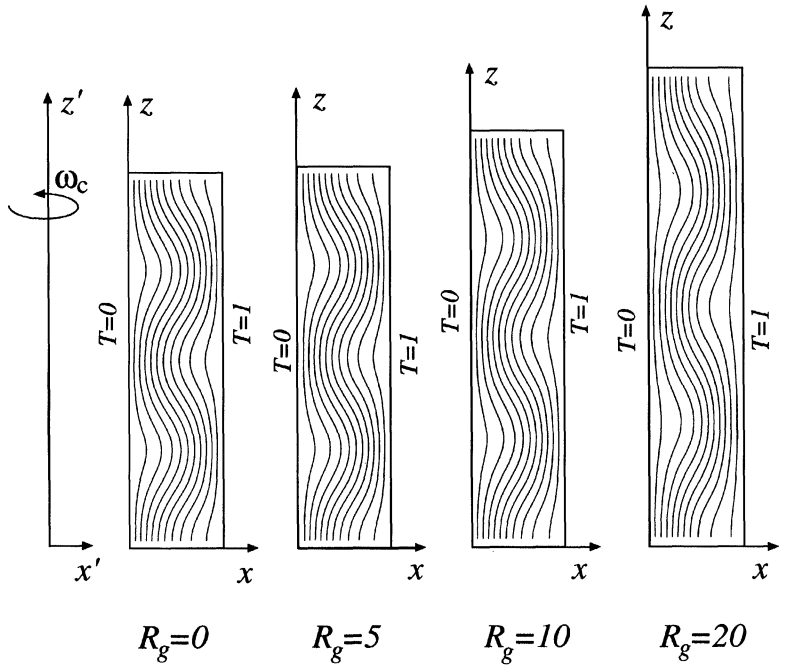

FIGURE 12 The convective temperature field at marginal stability for the odd modes corresponding to $A = 0.2$ and to four different values of $R_g = 0, 5, 10, 20$; isotherms equally divided between $T_{\min} = 0$ and $T_{\max} = 1$.

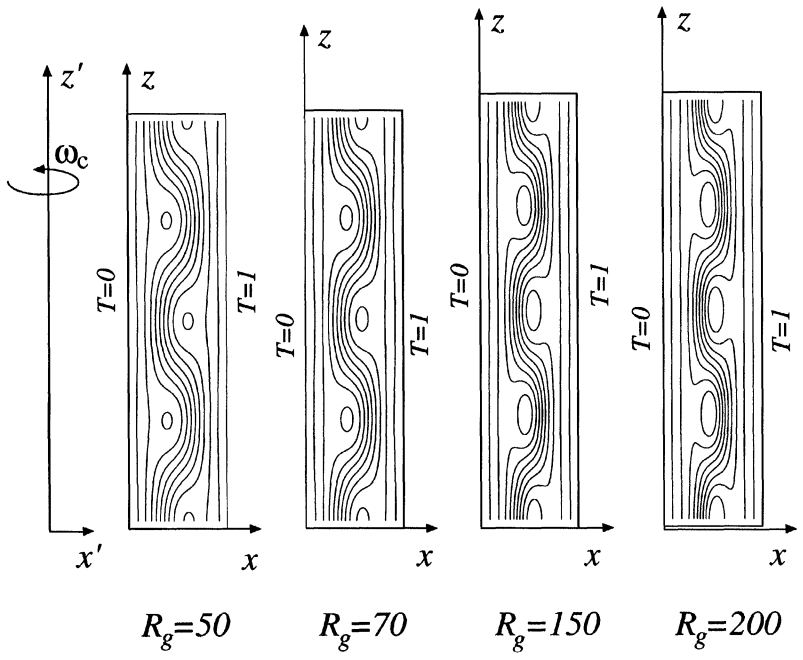

FIGURE 13 The convective temperature field at marginal stability for the odd modes corresponding to $A = 0.2$ and to four different values of $R_g = 50, 70, 150, 200$; isotherms equally divided between $T_{\min} = 0$ and $T_{\max} = 1$.

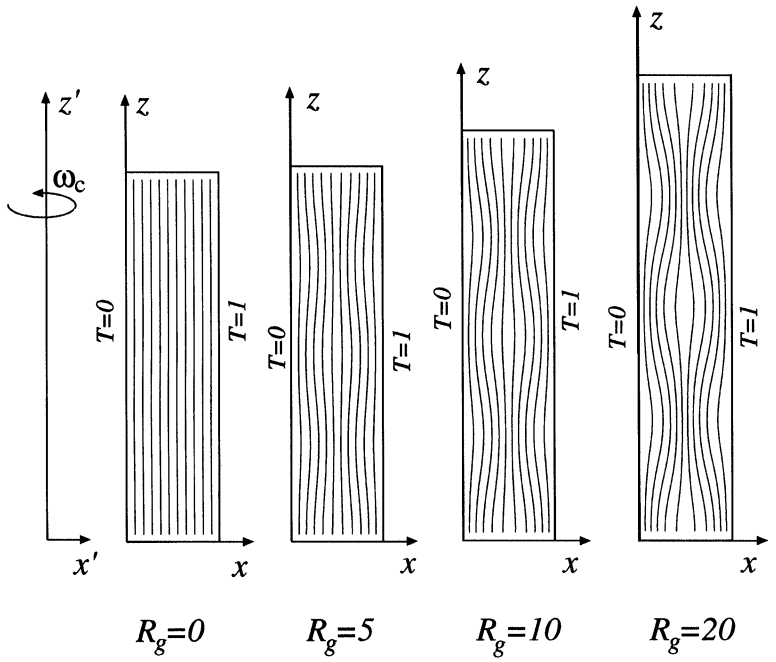

FIGURE 14 The convective temperature field at marginal stability for the even modes corresponding to $A = 0.2$ and to four different values of $R_g = 0, 5, 10, 20$; isotherms equally divided between $T_{\min} = 0$ and $T_{\max} = 1$.

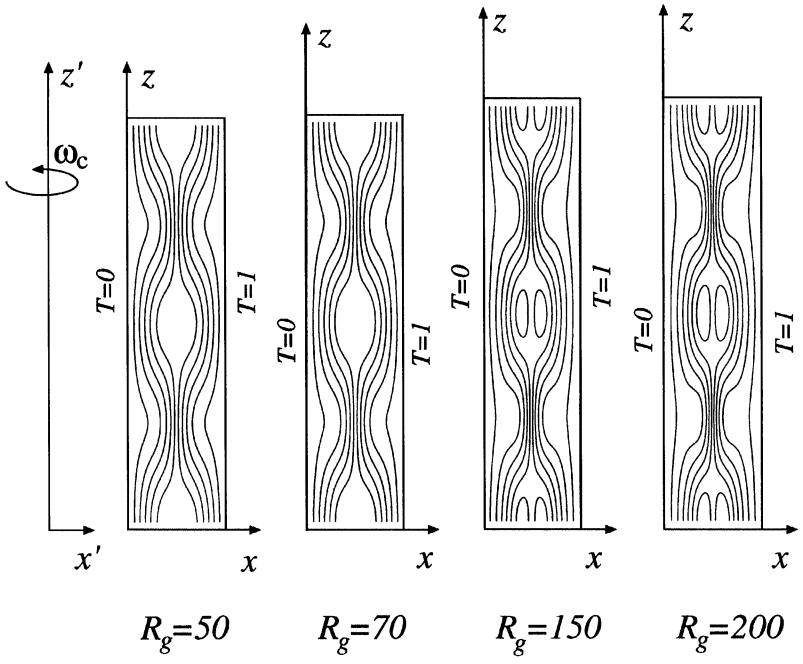

FIGURE 15 The convective temperature field at marginal stability for the even modes corresponding to $A = 0.2$ and to four different values of $R_g = 50, 70, 150, 200$; isotherms equally divided between $T_{\min} = 0$ and $T_{\max} = 1$.

figures indicating probably the effect of strong secondary circulation in these parts of the flow domain.

CONCLUSIONS

The effect of combined gravity and centrifugally driven convection in a rotating fluid saturated porous layer was investigated analytically. The linear stability analysis of the basic gravity driven convection shows that increasing the gravity related Rayleigh number has a stabilising effect on the basic flow. The resulting combined convection patterns seems to indicate different behaviour depending on the relative magnitude of the gravity related Rayleigh number as compared to the centrifugal Rayleigh number, the latter is expected to affect the amplitude of the convection at the perturbation level.

NOMENCLATURE

Latin Symbols

H = the front aspect ratio of the porous layer, equals H_*/L_*.
W = the top aspect ratio of the porous layer, equals W_*/L_*.
$\hat{e}_x$ = unit vector in the x direction.
$\hat{e}_y$ = unit vector in the y direction.
$\hat{e}_z$ = unit vector in the z direction.
$\hat{e}_n$ = unit vector normal to the boundary, positive outwards.
H_* = the height of the layer.
k_* = permeability of the porous domain.
L_* = the length of the porous layer.
M_f = a ratio between the heat capacity of the fluid and the effective heat capacity of the porous domain.
p = reduced pressure generalised to include the constant component of the centrifugal term (dimensionless).
$\boldsymbol{q}$ = dimensionless filtration velocity vector, equals $u\hat{e}_x + v\hat{e}_y + w\hat{e}_z$.
Ra_ω = porous media centrifugal Rayleigh number related to the contribution of the horizontal location within the porous layer to the centrifugal acceleration, equals $\beta_* \Delta T_c \omega_*^2 L_*^2 k_* M_f / \alpha_{e*} \nu_*$.
$Ra_{\omega 0}$ = porous media centrifugal Rayleigh number related to the contribution of the offset distance from the rotation centre to the centrifugal acceleration, equals $\beta_* \Delta T_c \omega_*^2 x_{0*} L_* k_* M_f / \alpha_{e*} \nu_*$.
$R_{\omega 0}$ = scaled centrifugal Rayleigh number, equals $Ra_{\omega 0}/\pi^2$.
T = dimensionless temperature, equals $(T_* - T_C)/(T_H - T_C)$.
T_C = coldest wall temperature.
T_H = hottest wall temperature.
u = horizontal x component of the filtration velocity.
v = horizontal y component of the filtration velocity.
w = vertical component of the filtration velocity.
W_* = the width of the layer.
x_0 = the dimensionless offset distance from the rotation centre, equals x_{0*}/L_*.
x = horizontal length coordinate.
y = horizontal width coordinate.
z = vertical coordinate.

Greek Symbols

α = a parameter related to the wave number, equals κ^2/π^2.
α_{e*} = effective thermal diffusivity.
β_* = thermal expansion coefficient.
γ = a parameter, equals κ_z/π.
δ_{ml} = Kronecker delta function.
η = the reciprocal of the offset distance from the rotation centre, equals $1/x_0 = Ra_\omega / Ra_{\omega 0}$.
ϕ = porosity.
ω_* = angular velocity of the rotating box.
ν_* = fluid's kinematic viscosity.
κ = wave number.

μ_* = fluid's dynamic viscosity.
ψ = stream function.
ΔT_c = characteristic temperature difference.

Subscripts

$*$ = dimensional values.
c = characteristic values.
cr = critical values.
tr = transitional values.
C = related to the coldest wall.
H = related to the hottest wall.

Acknowledgement

The authors would like to thank the Foundation for Research Development for partially funding this research through the Competitive Industry Research Grant (CIPM-GUN 2034039).

References

Bejan, A. (1995) Convection Heat Transfer, 2nd ed., Wiley, New York.

Jou, J.J. and Liaw, J.S. (1987a) "Transient Thermal Convection in a Rotating Porous Medium Confined between Two Rigid Boundaries", *Int. Communications in Heat and Mass Transfer*, Vol. 14, pp. 147–153.

Jou, J.J. and Liaw, J.S. (1987b) "Thermal Convection in a Porous Medium Subject to Transient Heating and Rotation", *Int.J. Heat Mass Transfer*, Vol. 30, pp. 208–211.

Nield, D.A. and Bejan, A. (1992) Convection in Porous Media, Springer Verlag, New York.

Patil, P.R. and Vaidyanathan, G. (1983) "On Setting Up of Convection Currents in a Rotating Porous Medium under the Influence of Variable Viscosity", *Int.J. Engineering Science*, Vol. 21, pp. 123–130.

Palm, E. and Tyvand, A. (1984) "Thermal Convection in a Rotating Porous Layer", *J. Appl. Math. & Physics* (*ZAMP*), Vol. 35, pp. 122–123.

Rudraiah, N., Shivakumara, I.S. and Friedrich, R. (1986) "The Effect of Rotation on Linear and Non-Linear Double-Diffusive Convection in Sparsely Packed Porous Medium", *Int.J. Heat Mass Transfer*, Vol. 29, No. 9, pp. 1301–1317.

Vadasz, P. (1993a) "Three-dimensional Free Convection in a Long Rotating Porous Box", *J. Heat Transfer*, Vol. 115, pp. 639–644.

Vadasz, P. (1993b) "Fluid Flow through Heterogeneous Porous Media in a Rotating Square Channel", *Transport in Porous Media*, Vol. 12, pp. 43–54.

Vadasz, P. (1994) "Stability of Free Convection in a Narrow Porous Layer Subject to Rotation", *Int. Comm. Heat Mass Transfer*, Vol. 21, No.6, pp. 881–890.

Vadasz, P. (1996a) "Stability of Free Convection in a Rotating Porous Layer Distant from the Axis of Rotation", *Transport in Porous Media*, Vol. 23, pp. 153–173.

Vadasz, P. (1996b) "Convection and Stability in a Rotating Porous Layer with Alternating Direction of the Centrifugal Body Force", *Int.J. Heat Mass Transfer*, Vol. 39, No. 8, pp. 1639–1647.

Wolfram, S. (1991) *Mathematica™: A System for Doing Mathematics by Computer* (2nd Edn), Wolfram Research Inc., Addison-Wesley Publishing Co., Redwood City – California.

MANEY
publishing

The Institute of Materials, Minerals & Mining

ENERGY MATERIALS

NEW FOR 2006

Materials Science & Engineering for Energy Systems

Maney Publishing on behalf of the Institute of Materials, Minerals and Mining

Economic and environmental factors are creating ever greater pressures for the efficient generation, transmission and use of energy. Materials developments are crucial to progress in all these areas: to innovation in design; to extending lifetime and maintenance intervals; and to successful operation in more demanding environments. Drawing together the broad community with interests in these areas, *Energy Materials* addresses materials needs in future energy generation, transmission, utilisation, conservation and storage. The journal covers thermal generation and gas turbines; renewable power (wind, wave, tidal, hydro, solar and geothermal); fuel cells (low and high temperature); materials issues relevant to biomass and biotechnology; nuclear power generation (fission and fusion); hydrogen generation and storage in the context of the 'hydrogen economy'; and the transmission and storage of the energy produced.

As well as publishing high-quality peer-reviewed research, *Energy Materials* promotes discussion of issues common to all sectors, through commissioned reviews and commentaries. The journal includes coverage of energy economics and policy, and broader social issues, since the political and legislative context influence research and investment decisions.

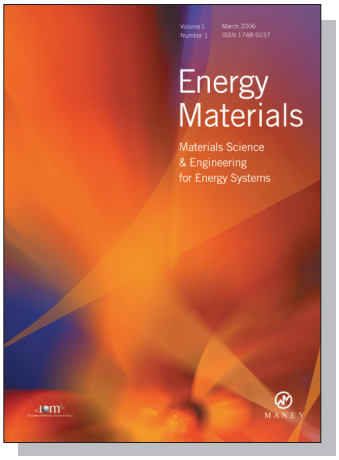

CALL FOR PAPERS

Contributions to the journal should be submitted online at **http://ema.edmgr.com**

To view the Notes for Contributors please visit: **www.maney.co.uk/journals/notes/ema**

Upon publication in 2006, this journal will be available via the Ingenta Connect journals service. To view free sample content online visit: **www.ingentaconnect.com/content/maney**

SUBSCRIPTION INFORMATION

Volume 1 (2006), 4 issues per year
Print ISSN: 1748-9237 Online ISSN: 1748-9245
Individual rate: £76.00/US$141.00
Institutional rate: £235.00/US$435.00
Online-only institutional rate: £199.00/US$367.00
For special IOM^3 member rates please email **subscriptions@maney.co.uk**

For further information please contact:
Maney Publishing UK
Tel: +44 (0)113 249 7481 Fax: +44 (0)113 248 6983 Email: subscriptions@maney.co.uk
or
Maney Publishing North America
Tel (toll free): 866 297 5154 Fax: 617 354 6875 Email: maney@maneyusa.com

For further information or to subscribe online please visit
www.maney.co.uk